NAG1-400

Thermal Effects on Cavity Stability of Cr:Nd:GSGG Laser Under Solar-Simulator Pumping

Ja H. Lee,

NASA Langley Research Center, Hampton, Virginia 23665-5225

Kyong H. Kim, Demetrius D. Venable and Lamarr A. Brown,

Department of Physics, Hampton University, Hampton, Virginia 23668

(NASA-TM-101273) THERMAL EFFECTS ON CAVITY STABILITY OF Cr:Nd:GSGG LASER UNDER SOLAR-SIMULATOR PUMPING (NASA) 30 p N90-70356

Unclas
00/36 0252413

Abstract

A chromium and neodymium co-doped gadolinium scandium gallium garnet (Cr:Nd:GSGG) crystal was tested for pulsed and continuous wave (CW) laser operations with a flashlamp and a solar-simulator as pumping sources. The crystal has been considered as a good candidate for a solar-pumped laser, since the broad absorption bands of the Cr^{3+}-sensitizer are located near the peak of the solar spectrum. CW laser operation lasting longer than 10 minutes was achieved at low solar-simulator pump power densities of up to 1,500 solar constants (203 W/cm^2). For higher pump power densitites of up to 2,500 solar constants (338 W/cm^2), a quasi CW laser operation was obtained with continuously chopped pumping with a duty cycle of 0.5 and repetition rate of 13 Hz. The experimental result was compared with the calculated stability condition of the laser resonator at various pump power densities and showed that the thermal focusing of the Cr:Nd:GSGG is more than 10 times greater than that of the neodymium-doped yttrium aluminum garnet (Nd:YAG) crystal laser.

I. Introduction

Solar-pumped continuous wave (CW) high power solid state lasers are being studied by NASA as a potential for laser-power transmission to various power users in space. Since the initial research on the solar-pumped solid state lasers done by Kiss and his coworkers[1] in the early 1960's, there have been a number of papers published on the subject. The highest laser output reported was about 100 W CW from a neodymium-doped yttrium aluminum garnet (Nd:YAG) crystal pumped with a solar furnace.[2] So far, the Nd:YAG crystal has been demonstrated to be the best solid state laser material under solar pumping because of its superior characteristics on thermal conductivity, uniformity of ion concentration in host material, high quantum efficiency, and mechanical strength compared with other host crystals.

However, one disadvantage of the Nd:YAG crystal is that the use of the solar beam as a pumping source is very inefficient. It has narrow absorption bands over the solar spectrum region. In order to make efficient use of the solar spectrum, an idea utilizing the broad absorption spectrum of the chromium ions in the visible spectral region was initiated, and the chromium (Cr^{3+})-sensitized Nd:YAG crystal was first investigated under solar pumping by Reno in 1966.[3] He observed that the Cr-ions do not improve the laser action of the Nd:YAG because of the slow energy transfer rate from Cr^{3+} to Nd^{3+} ions. In 1982, a new crystal, Cr:Nd:GSGG (chromium and neodymium co-doped gadolinium scandium gallium garnet), was introduced and was shown to provide an efficient energy transfer from chromium to neodymium ions.[4,5] Lasing properties of the Cr:Nd:GSGG crystal have been tested by several research groups,[5-8] and they have shown that its slope efficiency is twice that of Nd:YAG in pulsed operations. Because of this advantage, the Cr:Nd:GSGG crystal has been considered as a lasant material for the solar-pumped laser, and its CW laser operation has been tested with a solar-simulator as a pumping source in this research. The stability condition of our specific laser resonator, which was affected by the thermal lensing effect, was calculated and compared with the experimental results.

II. Flashlamp Experiment

Before studying the CW laser operation, performances of the Cr:Nd:GSGG crystal in short- and long-pulsed flashlamp pumping were studied and compared with that of the Nd:YAG. Figure 1 shows a schematic diagram of the system used. Each Cr:Nd:GSGG and Nd:YAG crystal, whose sizes are 3.2 mm in diameter and 76 mm in length, had anti-reflection coatings at both ends and was placed at one focus of an elliptical cavity along with a xenon flashlamp placed at the second focus. The laser cavity was 0.3-m long and consisted of a highly reflective mirror with a 5-m curvature and a 95-percent reflective mirror with a flat surface. A pyroelectric energy meter was used to measure the laser output energy and the optical energy of the flashlamp emission, and silicon photodiodes were used to monitor the laser and the pump pulses.

In order to vary the pulse length of the flashlamp, the capacitance and inductance of the electrical circuit were changed to various values. Three different pulse widths were used in this experiment; typical pump and laser pulses are shown in Figure 2. Graphs showing laser output energy as a function of total optical energy from the flashlamp are shown in Figures 3(a)-(c), and the corresponding slope efficiencies and thresholds are listed in Table 1. The threshold is determined as the extrapolated intercept for the linear portion of the data shown in the figures. The slope efficiency for Cr:Nd:GSGG was greater than that of the Nd:YAG in the three different pulse widths and increased as the pulse width increased. The Cr:Nd:GSGG crystal used in this flashlamp experiment had a dopant concentration of $2x10^{20}$ ions/cm^3 for each of the Cr^{3+} and Nd^{3+} ions, and the Nd:YAG crystal had a $1.52x10^{20}$ Nd^{3+} ions/cm^3 doping density.

III. CW Laser Experiment

In CW operation a solar-simulator consisting of a Xe-arc lamp and an elliptical reflector was used as shown in Figure 4. The spectrum of the solar simulator beam resembles the air mass-zero solar spectrum except for a couple of xenon emission lines at about 760 and 830 nm. The simulator beam was converged by a conical aluminum collector along the axis of the laser rod. Both the Cr:Nd:GSGG and Nd:YAG crystals had the same dopant concentrations and the same dimensions as those used for the flashlamp pump experiment, except the crystals used here had highly reflective mirrors with a curvature of 5-m radius coated at one of their ends. The water-jacket glass tube, having an outside diameter of 160 mm and inner diameter of 140 mm, was used for cooling the laser rod. The resonator length was 165 mm, and the output mirror had 98 percent reflectivity at 1.06 μm, 0.30 m radius of curvature, and 1" diameter.

For the Nd:YAG crystal, continuous laser operation was observed with the pump power density from 200 solar constants (27 W/cm^2) to 3000 solar constants (406 W/cm^2). However, for the Cr:Nd:GSGG crystal, the laser cavity remained stable, and CW lasing was possible only when the pump power density was not greater than 1,500 solar constants (203 W/cm^2). Figure 5 shows the typical laser signal of the Cr:Nd:GSGG that terminates in less than 1 at pump power density of 2,500 solar constants.

When the chopper was used to pulse the pump beam for the Cr:Nd:GSGG laser at high pump power densities, continuously pulsed lasing was achieved at various chopper speeds from 0.6 Hz to 13 Hz. The ratio of the chopper's open-to-closed sections was one, the duty cycle was 0.5, and the pumping duration was 0.35 s at 0.7 Hz. The lasing lasted as long as the chopped pump period. Figures 6(a) and 6(b) show the laser outputs for the chopped pumping. The stable quasi-CW laser operation as shown was possible at pump power densities below 2,500 solar constants (338 W/cm^2), at which the peak laser output power was about 340 mW and the corresponding average power was 170 mW. However, for a pump power density of 3,000 solar constants (405 W/cm^2), even the quasi CW lasing became unstable and disappeared 1.5 s after initial lasing.

IV. Thermal Focus and Cavity Stability

The absorbed pump power P_a by a crystal rod is written as

$$P_a = \int_{z=0}^{L} \int_{0}^{2\pi} \int_{\lambda_1}^{\lambda_2} I_o(\lambda,\phi,z)\,[1 - \exp\{-\varepsilon(\lambda)s\}]d\lambda\;(1 - \xi)\;r_o d\phi\;dz \tag{1}$$

where $I_o(\lambda,\phi,z)$ is the spectral irradiance of the pump light at the rod surface (W/cm^2), $\varepsilon(\lambda)$ is the absorption coefficient of the crystal at the given wavelength λ(cm^{-1}) , s is the path length of the pump beam in the crystal (cm) and a constant for the integration, ξ is the reflective loss coefficient for the pump beam at the rod surface, r_o is the rod radius (cm) and L is the length of rod (cm). The absorption spectrum of the Cr:Nd:GSGG crystal is compared with the solar spectrum in Figure 7, and the solar-simulator's beam profile along the crystal axis is shown in Figure 8. The pump beam power absorbed by the crystal causes a radial temperature gradient which can be obtained by solving the one-dimensional heat conduction equation[9]:

$$T(r) = T(r_o) + \frac{P_a}{4\pi\, r_o^2\, K\, L}\,(r_o^2 - r^2) \tag{2}$$

where K is the thermal conductivity of the crystal. Thus, the temperature difference between the rod surface and rod center is written as

$$T(0) - T(r_o) = \frac{P_a}{4\pi\, K\, L} \tag{3}$$

This radial temperature gradient generates mechanical stresses in the laser rod and introduces variation in the refractive index. The combined effect of a temperature- and a stress-dependent variation of the refractive index is expressed as [9,10]

$$\begin{aligned} n(r) &= n_o + \Delta n(r) \\ &= n_o\left[1 - \frac{P_a}{2\pi\, r_o^2\, K\, L}\left(\frac{1}{2n_o}\frac{dn}{dT} + n_o^2 \alpha\, C_{r,\phi}\right) r^2\right] \end{aligned} \tag{4}$$

where n_o is the index of refraction of the crystal, α is the linear thermal expansion coefficient, and C_r and C_ϕ are the elasto-optic constants for light with radial and tangential polarization. This radial variation of the refractive index makes the crystal behave like a lens-like medium.

From the theoretical derivation shown in the Appendix, we obtain an equation for the focal length due to thermal lensing effects caused by the radial variation of the refractive index as

$$f = [\frac{2n_o}{b} \sin \frac{2L}{b}]^{-1} \tag{5}$$

and the cavity parameters for our laser resonator as

$$G_1 = \frac{a_1}{a_2} [\cos \frac{2L}{b} - \frac{2n_o d}{b} \sin \frac{2L}{b} - \frac{1}{R_1}(\frac{b}{2} \sin \frac{2L}{b} + n_o d \cos \frac{2L}{b})] \tag{6}$$

$$G_2 = \frac{a_2}{a_1} [n_o \cos \frac{2L}{b} - \frac{1}{R_2} (\frac{b}{2} \sin \frac{2L}{b} + n_o d \cos \frac{2L}{b})] \tag{7}$$

where d is the distance from the flat end of the rod to the output mirror and b is the measure of the degree of variation of n and can be expressed as

$$b = [\frac{P_a}{4\pi r_o^2 K L} (\frac{1}{2n_o} \frac{dn}{dT} + n_o^2 \alpha C_{r,\phi})]^{-1/2} \tag{8}$$

The mirror diameters are $2a_1$ and $2a_2$, respectively, and the corresponding radii of curvatures are R_1 and R_2 which are illustrated in Figure 9. Then, the resonator stability condition is specified in the following form:

$$-1 < G_1 \cdot G_2 < 1 \tag{9}$$

Table 2 lists the parameters used in the calculation, and some of them were obtained from Refs. 11 and 12. Table 3 shows the calculated values of absorbed pump power in the crystals, the temperature difference between the center and surface of both Cr:Nd:GSGG and Nd:YAG laser rods, thermal focusing, and resonator stability condition at various CW pump powers densities. The large temperature difference between the surface and center of the Cr:Nd:GSGG rod causes severe thermal focusing compared with the Nd:YAG's case even at low pump powers. The ratio of the thermal focusing powers of the two rods, $[1/f(GSGG)]/[1/f(YAG)]$, decreases from 15 to 8 as the pump power density increases from 1,000 solar constants to 3,000 solar constants. These numbers are greater than those discussed in Refs. 7 and 8. Whereas the laser resonator of the Nd:YAG crystal stays stable for pump power densities greater than 3,000 solar constants, that of the Cr:Nd:GSGG crystal is stable only up to 1,500 solar constants. The experimental results agree with these calculations. The distortion of the end-face curvature of the rod caused by the radial temperature gradient was neglected in our calculation because both ends of the rod were placed in regions shaded from the pump beam, as shown in Figure 4. The difficulty of the CW laser operation of the Cr:Nd:GSGG experiment was also observed by Barnes, et al. in Ref. 13.

V. Conclusion

Our results show that the slope efficiency of the Cr:Nd:GSGG crystal is higher than that of the Nd:YAG crystal in various pulse widths (0.11 ms, 0.28 ms and 0.90 ms) for a flashlamp pumped experiment, and increases as the pulse width increases. When the solar simulator was used as the pumping source, the CW laser operation of the Cr:Nd:GSGG crystal was limited, whereas the Nd:YAG successfully performed for all pump power densities available. True CW laser operations of the Cr:Nd:GSGG were observed for pump power densities less than or equal to 1500 solar constants (230 W/cm^2). For pump power densities above 1,500 solar constants to 2,500 solar constants (338 W/cm^2), a quasi-CW laser operation was demonstrated. Our calculations show that the solar beam absorption by the Cr:Nd:GSGG is about six times larger than that by the Nd:YAG for the same incoming beam, and thermal focusing power of the Cr:Nd:GSGG is 15- to 8-times greater than that of the Nd:YAG for the pump power densities from 1,000 to 3,000 solar contants. The Cr:Nd:GSGG crystal was damaged by thermal cracking when the quasi-CW laser operation was performed at the pump power density of 3,000 solar constants (405 W/cm^2) for several minutes. We found that better solar-pumped laser performance of the Cr:Nd:GSGG over Nd:YAG expected in past studies may be difficult to realize with the rod geometry. However, a fiber bundle of the Cr:Nd:GSGG crystal, if available, can possibly solve the thermal problems with a proper water cooling.

Appendix

According to Refs. 14 and 15, the ray matrix relating the output ray (x_2, x'_2) to the input ray (x_0, x'_0) in a lens-like medium whose refractive index n varies near the optical axis as in $n = n_0 (1 - 2 r^2/b^2)$ is written, using the notations shown in Figure 9, as

$$\begin{vmatrix} x_2 \\ x'_2 \end{vmatrix} = \begin{vmatrix} 1 & 0 \\ 0 & n_0 \end{vmatrix} \begin{vmatrix} x_1 \\ x'_1 \end{vmatrix}$$

$$= \begin{vmatrix} 1 & 0 \\ 0 & n_0 \end{vmatrix} \begin{vmatrix} \cos(2L/b) & (b/2)\sin(2L/b) \\ -(2n_0/b)\sin(2L/b) & n_0\cos(2L/b) \end{vmatrix} \begin{vmatrix} x_0 \\ x'_0 \end{vmatrix}$$

where n_0 is a constant, b is the measure of the degree of the variation of n, and L is the distance between the input and output ray points in the lens-like medium. For the resonator shown in Figure 9, the output ray (x_3, x'_3) at the output mirror is related to the input ray (x_0, x'_0) by the combination of the above ray matrix and a ray matrix in a free space:

$$\begin{vmatrix} x_3 \\ x'_3 \end{vmatrix} = \begin{vmatrix} 1 & d \\ 0 & 1 \end{vmatrix} \begin{vmatrix} x_2 \\ x'_2 \end{vmatrix}$$

$$r = \begin{vmatrix} 1 & d \\ 0 & 1 \end{vmatrix} \begin{vmatrix} \cos(2L/b) & (b/2)\sin(2L/b) \\ -(2n_0/b)\sin(2L/b) & n_0\cos(2L/b) \end{vmatrix} \begin{vmatrix} x_0 \\ x_0' \end{vmatrix}$$

$$= \begin{vmatrix} \cos(2L/b)-(2n_0 d/b)\sin(2L/b) & (b/2)\sin(2L/b)+n_0 d\cos(2L/b) \\ -(2n_0/b)\sin(2L/b) & n_0\cos(2L/b) \end{vmatrix} \begin{vmatrix} x_0 \\ x_0' \end{vmatrix}$$

$$= \begin{vmatrix} A & B \\ C & D \end{vmatrix} \begin{vmatrix} x_0 \\ x_0' \end{vmatrix}$$

where $A = \cos(2L/b) - (2n_0 d/b)\sin(2L/b)$

$B = (b/2)\sin(2L/b) + n_0 d\cos(2L/b)$

$C = -(2n_0/b)\sin(2L/b)$

$D = n_0\cos(2L/b)$

Thus, the focal length of the lens-like medium is written as

$$f \equiv -1/C = [(2n_0/b)\sin(2L/b)]^{-1}$$

and cavity parameters G of the optical resonator shown in Figure 9 are written as

$$G_1 = (a_1/a_2)\ (A - B/R_1)$$

$$= (a_1/a_2)\ [\cos(2L/b) - (2n_0 d/b)\sin(2L/b) - \{(b/2)\sin(2L/b) + n_0 d\ \cos\ (2L/b)\}/R_1]$$

$$G_2 = (a_1/a_2)\ (D - B/R_2)$$

$$= (a_1/a_2)\ [n_0\cos(2L/b) - \{(b/2)\sin(2L/b) + n_0 d\ \cos(2L/b)\}/R_2]$$

It was found during the course of this research that a similar analysis was done for the Nd:YAG crystal in Ref. 16, and the refractive index of the crystal was incorrectly placed in parts of their equations.

Acknowledgement

The authors wish to thank Michael T. Stubbs for his technical assistance. This work is supported in part by NASA under grant numbers NAG-1-441 and NAG-1-400.

References

1. Z. J. Kiss, H. R. Lewis, and R. C. Duncan, Appl. Phys. Lett. 2 (5), 93(1963).

2. M. Weksler and J. Shwartz, SPIE vol. 736, New Slab and Solid-State Laser Technologies and Applications, 84 (1987).

3. G. W. Reno, RCA Review, page 149, March 1966.

4. A. Beimowski, G. Huber, D. Pruss, V. V. Laptev, J. A. Shcherbakov, and Y. V. Zharikov, Appl. Phys. B 28, 234 (1982).

5. D. Pruss, G. Huber, A. Beimowski, V. V. Laptev, J. A. Shcherbakov, and Y. V. Zharikov, Appl. Phys. B 28, 355 (1982).

6. E. V. Zharikov, et. al., Sov. J. Quantum Electron. 14 (10), 1306 (1983).

7. E. Reed, IEEE J. Quantum Electron. QE-21 (10), 1625 (1985).

8. S. E. Stokowski, SPIE Vol. 736 New Slab and Solid-State Tech. & Appl., 22 (1987).

9. W. Koechner, "Solid State Laser Engineering," Springer-Verlag, New York, (1987), chapter 7.

10. J. D. Foster and L. M. Osterink, J. Appl. Phys., 41 (9), 3656 (1970).

11. Allied Corporation, Synthetic Crystal Products Data Sheet, P. O. Box 31428 Charlotte, North Carolina 28231 (1986).

12. W. F. Krupke, M. D. Shinn, J. E. Marion, J. A. Caird, and S. E. Stokowskii J. Optical Soc. Am. B, 3 (1), 102 (1986).

13. N. P. Barnes, D. J. Gettemy, L. Esterowitz, and R. E. Allen, IEEE J. Quantum Electron. QE-23 (9), 1434 (1987).

14. H. Kogelnik, The Bell System Tech. Journal, 44, 455 (1965).

15. A. Yariv, "Quantum Electronics," 2nd ed. John Wiley & Sons, New York (1975), Chapter 6.

Figure Captions

Fig. 1 Schematic diagram of the experimental setup for flashlamp pumped laser experiment. PD-silicon photodiode; M1 and M2-laser cavity mirrors.

Fig. 2 Typical laser (upper trace) and pump beam (lower trace) signals obtained in the long-pulsed flashlamp pumped laser measurement.

Fig. 3(a) Comparision of Cr:Nd:GSGG and Nd:YAG lasers pumped by a short-pulsed flashlamp.

Fig. 3(b) Comparision of Cr:Nd:GSGG and Nd:YAG lasers pumped by a relatively long-pulsed flashlamp.

Fig. 3(c) Comparision of Cr:Nd:GSGG and Nd:YAG lasers pumped by longest-pulsed flashlamp.

Fig. 4 Experimental setup used for CW and chopped operations of Cr:Nd:GSGG lasers with a solar-simulator as a pumping source. PD-silicon photodiode.

Fig. 5 Typical laser (upper trace) and pump beam (lower trace) signals of the Cr:Nd:GSGG laser pumped by the solar-simulator's high pump power densities (greater than 1,500 solar constants).

Fig. 6(a) Quasi-CW laser signals (upper trace) and chopped pump beam signals (lower trace) of the Cr:Nd:GSGG laser at high pump power densities.

Fig. 6(b) The long time operation of the quasi-CW laser of the Cr:Nd:GSGG crystal at high pump power densities.

Fig. 7 Absorption spectrum of the Cr:Nd:GSGG crystal (solid line) and the air-mass-zero solar spectrum (dotted line). The concentrations of the Cr^{3+}- and Nd^{3+}-ions are the same, 2×10^{20} ions/cm^3.

Fig. 8 Solar-simulator beam distribution along collector cone axis where laser rod is placed. Dotted line indicates position of the rod.

Fig. 9 Diagram showing the ray position (x) and direction (x') with respect to the central axis at various positions in the laser cavity used in the CW laser operation. $2a_1$ and $2a_2$ are the diameters of the mirrors, and R_1 and R_2 are the radii of the mirror curvatures.

Table 1. Results of the flashlamp experiment with Cr:Nd:GSGG and Nd:YAG crystals for various pump pulse widths.

Capacitance (μF)	Inductance (mH)	Pulse Width (ms)	Threshold (J) GSGG	YAG	Slope Efficiency (%) GSGG	YAG
25	0	0.09 - 0.13	0.99	0.73	1.25	0.75
75	0	0.13 - 0.43	1.64	1.61	1.59	1.24
75	3.8	0.89 - 0.91	1.97	1.68	1.70	1.32

Table 2. Thermal and Physical Parameters of Cr:Nd:GSGG and Nd:YAG

	Cr:Nd:GSGG	Nd:YAG	Reference
n_0	1.95	1.82	11
α (x 10^{-6}/K)	7.5	7.5	11
dn/dT (x 10^{-6}/K)	10.1	7.3	11
K (W/cm-K)	0.06	0.14	11
C_r	0.024	0.0196	12
C_ϕ	0.0015	-0.0025	12
r_0 (cm)	0.16	0.16	
L (cm)	7.62	7.62	
a_1 (cm)	0.16	0.16	
a_2 (cm)	1.27	1.27	
R_1 (cm)	500	500	
R_2 (cm)	30	30	
d (cm)	9.0	9.0	
ξ	0.02	0.02	
s (cm)	0.343	0.347	
λ_1 (cm)	300	300	
λ_2 (nm)	900	900	

Note:
1. The rod length L was replaced in the absorbed pump power calculations with the length of rod exposed to the pump light which is about 6.9 cm.
2. The value for reflective loss coefficient, ξ , at the rod surface was approximated.
3. The path length of the pump beam in the crystal is calculated as $s=2r_0/\cos[\sin^{-1}(\sin 45°/n_0)]$ for a 45° incident light.

Table 3. Absorbed pump power in the crystals, temperature difference between center and surface of laser rod, thermal focus, and stability condition

SOLAR CONSTANT	ABSORBED POWER	T(0) - T(R) ^{o}C	F_r (cm)	F_ϕ (cm)	$G_2 - G_2$	STABILITY CONDITION
Cr:Nd:GSGG						
1000	330.21	57.47	3.10		0.45	STABLE
				3.62	0.70	STABLE
1500	495.32	86.21	2.44		0.74	STABLE
				2.75	0.03	STABLE
2000	660.42	114.95	2.20		2.21	UNSTABLE
				2.37	1.05	UNSTABLE
2500	825.53	143.69	2.15		3.52	UNSTABLE
				2.20	2.24	UNSTABLE
3000	990.64	172.42	2.24		4.44	UNSTABLE
				2.15	3.31	UNSTABLE
Nd:YAG						
1000	55.21	4.12	45.66		.69	STABLE
				58.36	.75	STABLE
1500	82.82	6.18	30.68		.56	STABLE
				39.15	.64	STABLE
2000	110.42	8.24	23.19		.43	STABLE
				29.54	.54	STABLE
2500	138.03	10.30	18.70		.32	STABLE
				23.78	.45	STABLE
3000	165.64	12.36	15.71		.21	STABLE
				19.94	.36	STABLE

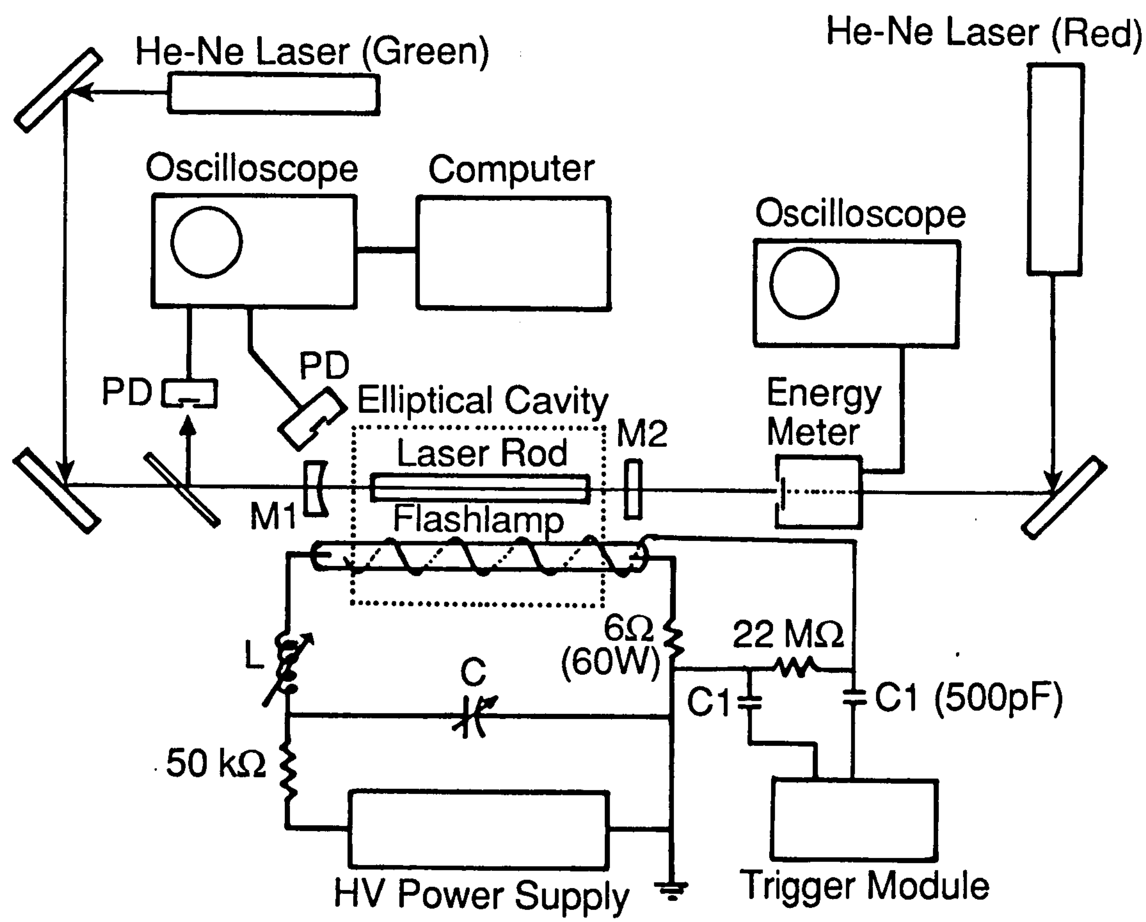
He-Ne Laser (Green)
He-Ne Laser (Red)
Oscilloscope
Computer
Oscilloscope
PD
PD
Elliptical Cavity
M2
Laser Rod
M1
Flashlamp
Energy
Meter
6Ω
(60W)
22 MΩ
L
C
C1
C1 (500pF)
50 kΩ
HV Power Supply
Trigger Module

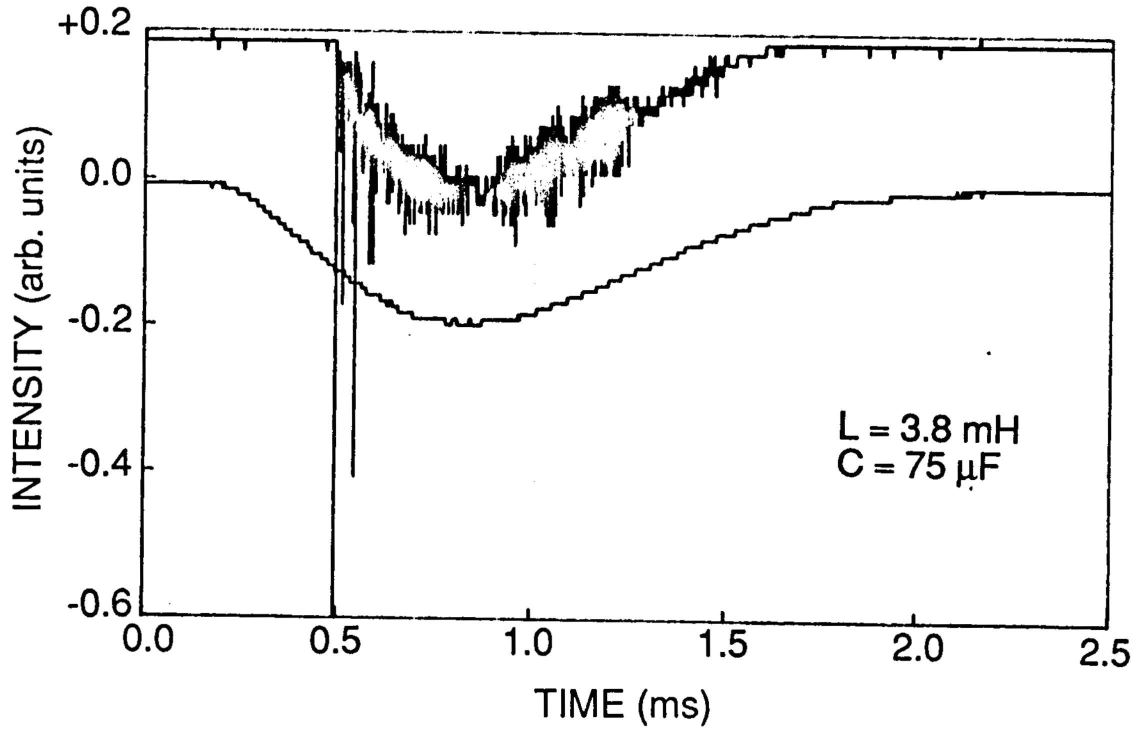

+0.2
0.0
-0.2
-0.4
-0.6
INTENSITY (arb. units)
0.0
0.5
1.0
1.5
2.0
2.5
TIME (ms)
L = 3.8 mH
C = 75 μF

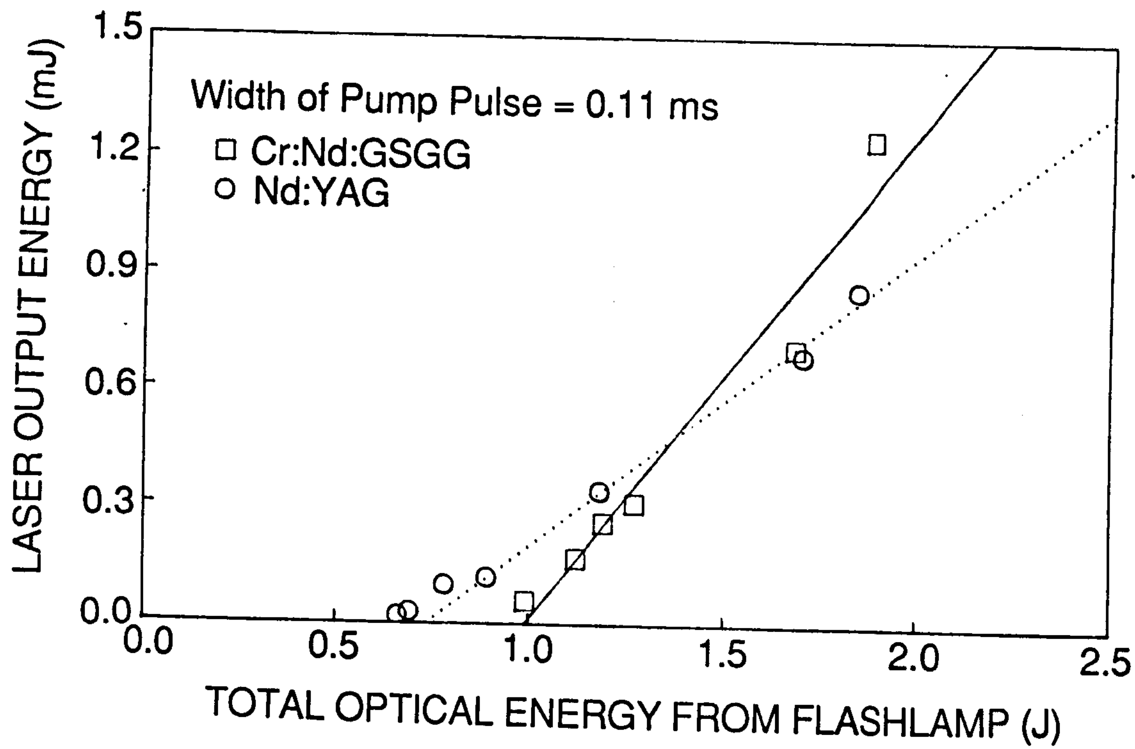
Width of Pump Pulse = 0.11 ms
Cr:Nd:GSGG
Nd:YAG
LASER OUTPUT ENERGY (mJ)
TOTAL OPTICAL ENERGY FROM FLASHLAMP (J)
0.0
0.3
0.6
0.9
1.2
1.5
0.0
0.5
1.0
1.5
2.0
2.5

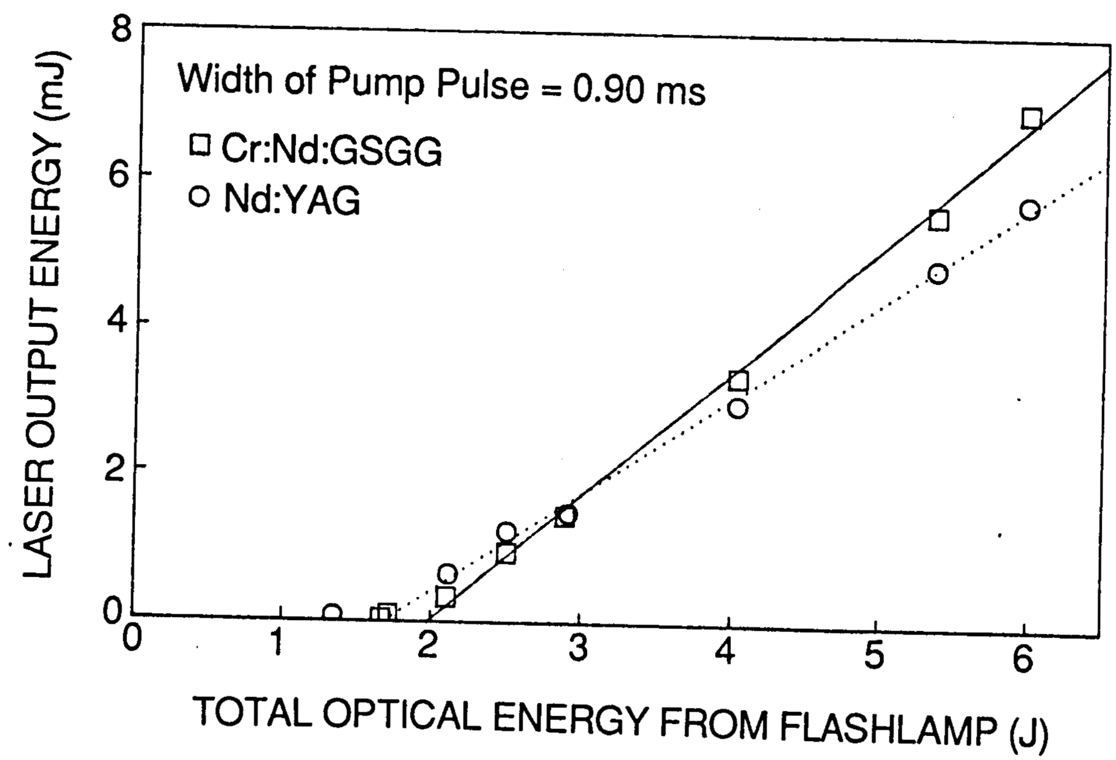
Width of Pump Pulse = 0.90 ms
Cr:Nd:GSGG
Nd:YAG
LASER OUTPUT ENERGY (mJ)
TOTAL OPTICAL ENERGY FROM FLASHLAMP (J)
0
2
4
6
8
0
1
2
3
4
5
6

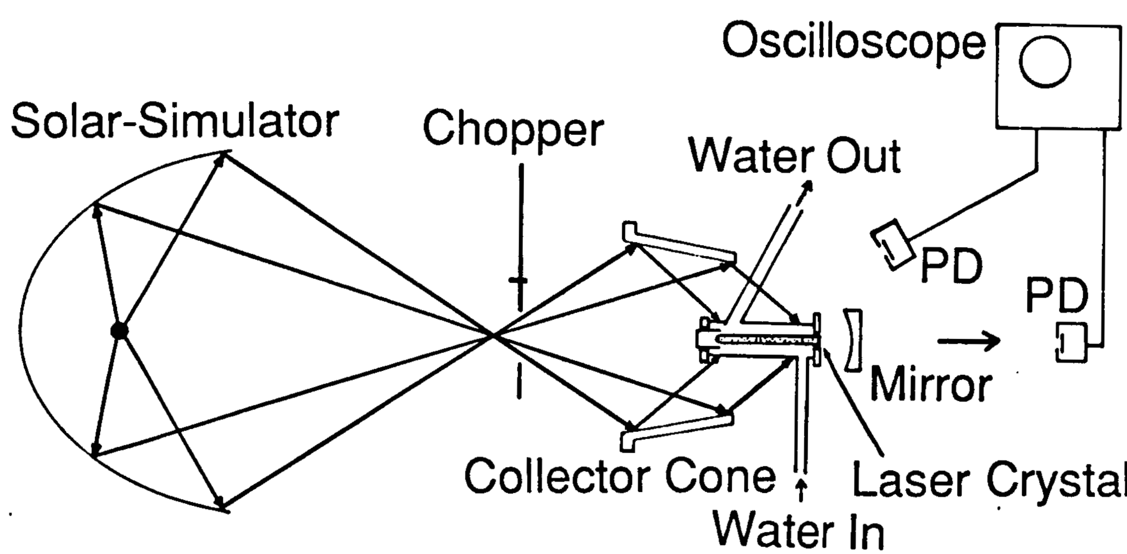

Oscilloscope
Solar-Simulator
Chopper
Water Out
PD
PD
Mirror
Collector Cone
Laser Crystal
Water In

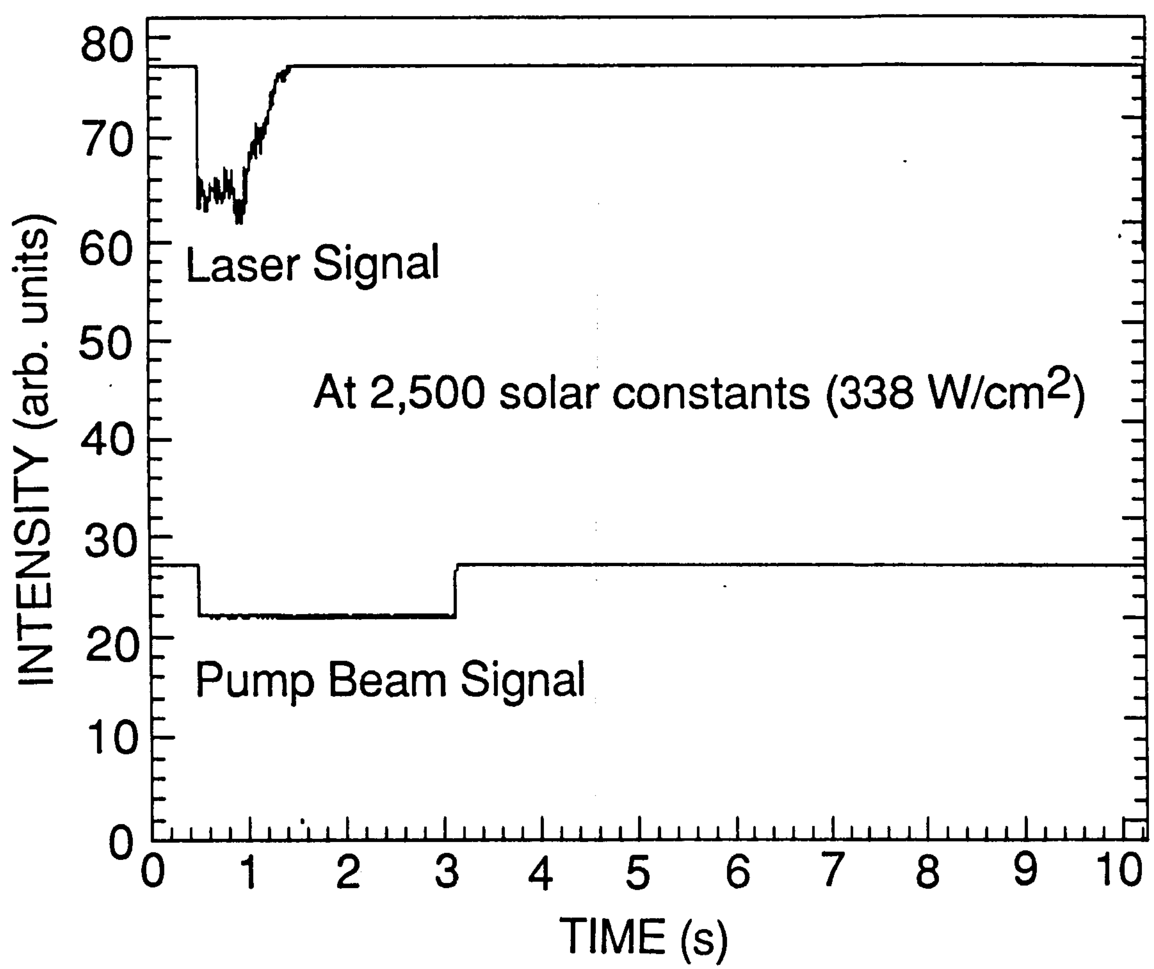

INTENSITY (arb. units)
80
70
60
50
40
30
20
10
0
Laser Signal
At 2,500 solar constants (338 W/cm2)
Pump Beam Signal
0
1
2
3
4
5
6
7
8
9
10
TIME (s)

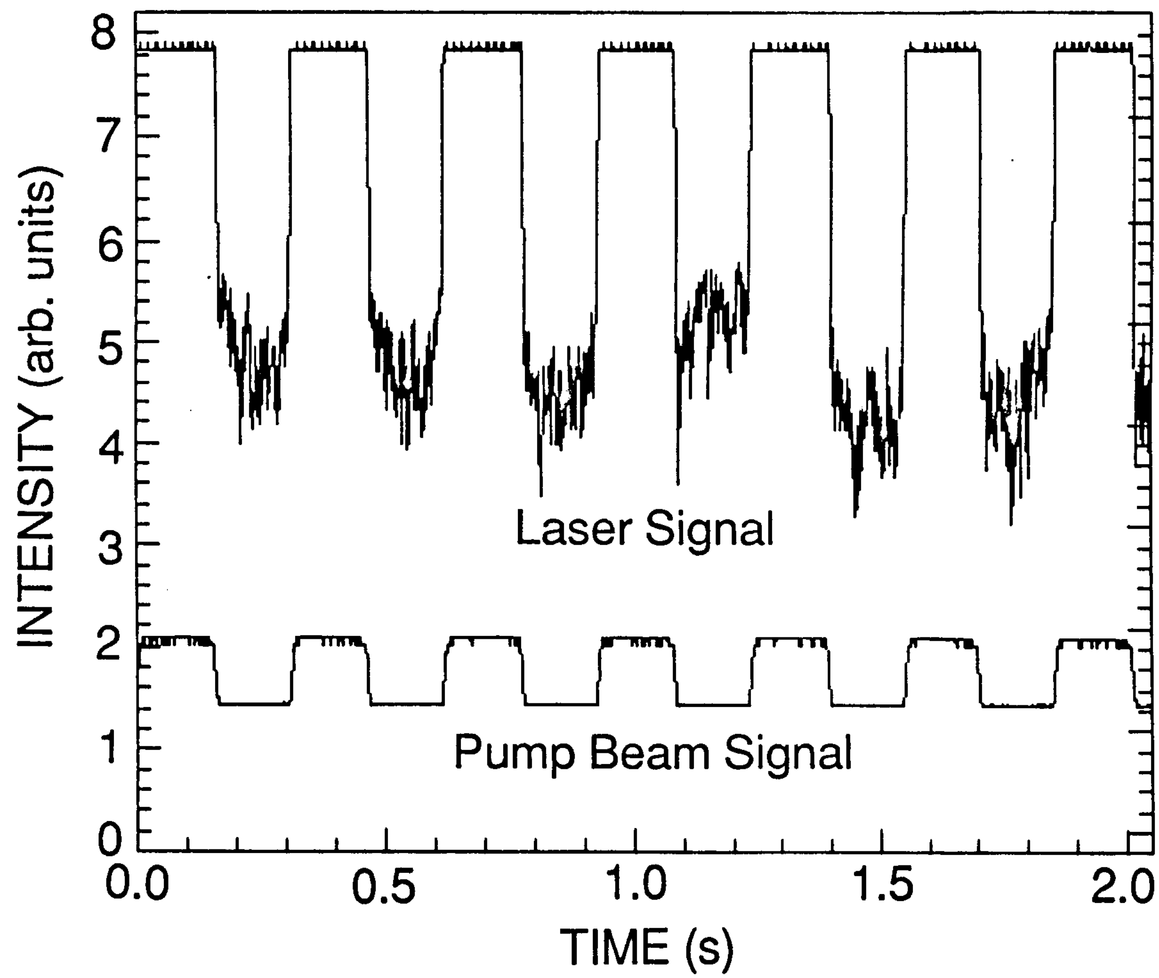
Laser Signal
Pump Beam Signal
INTENSITY (arb. units)
TIME (s)
0
1
2
3
4
5
6
7
8
0.0
0.5
1.0
1.5
2.0

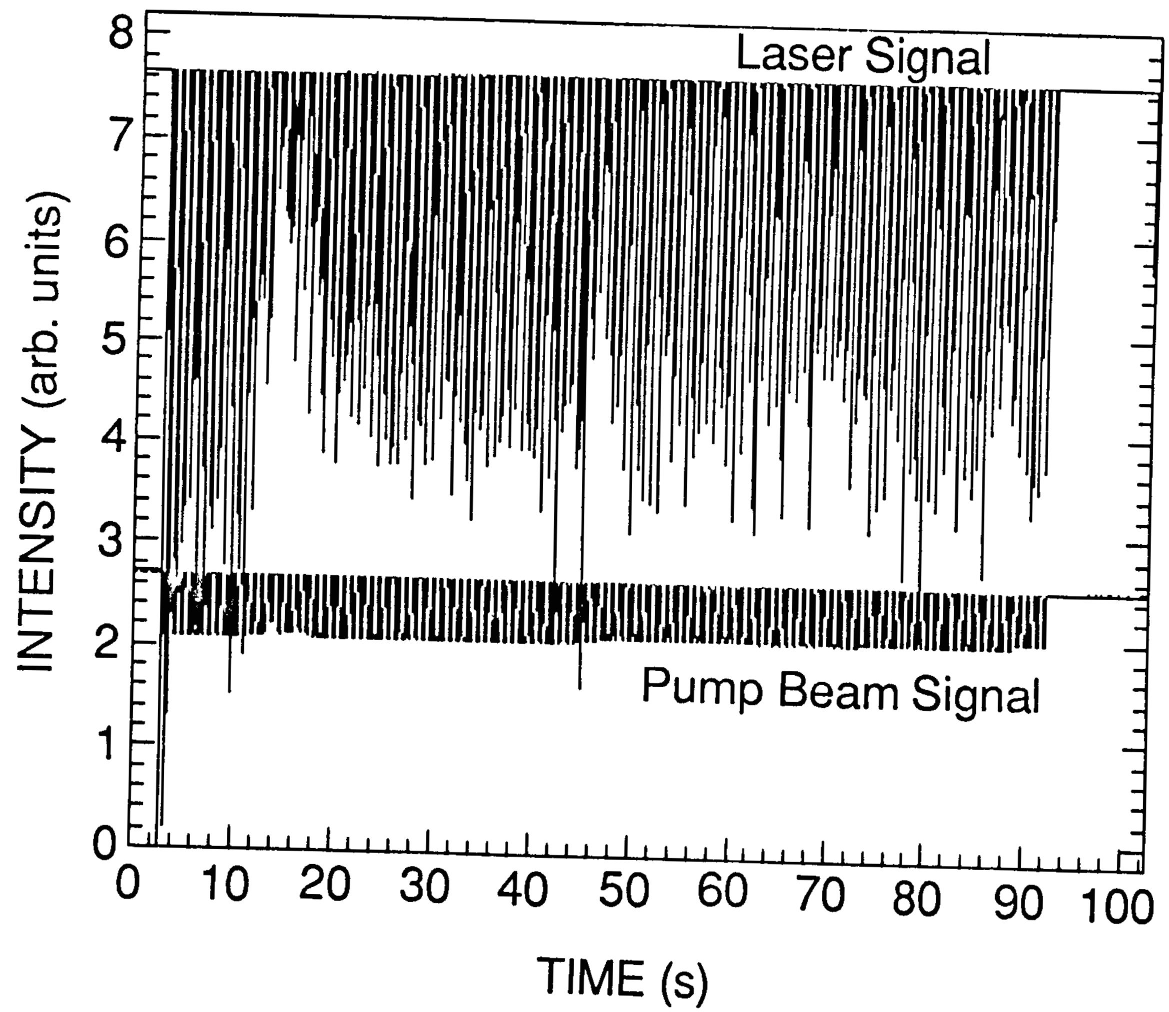
Laser Signal
Pump Beam Signal
INTENSITY (arb. units)
TIME (s)

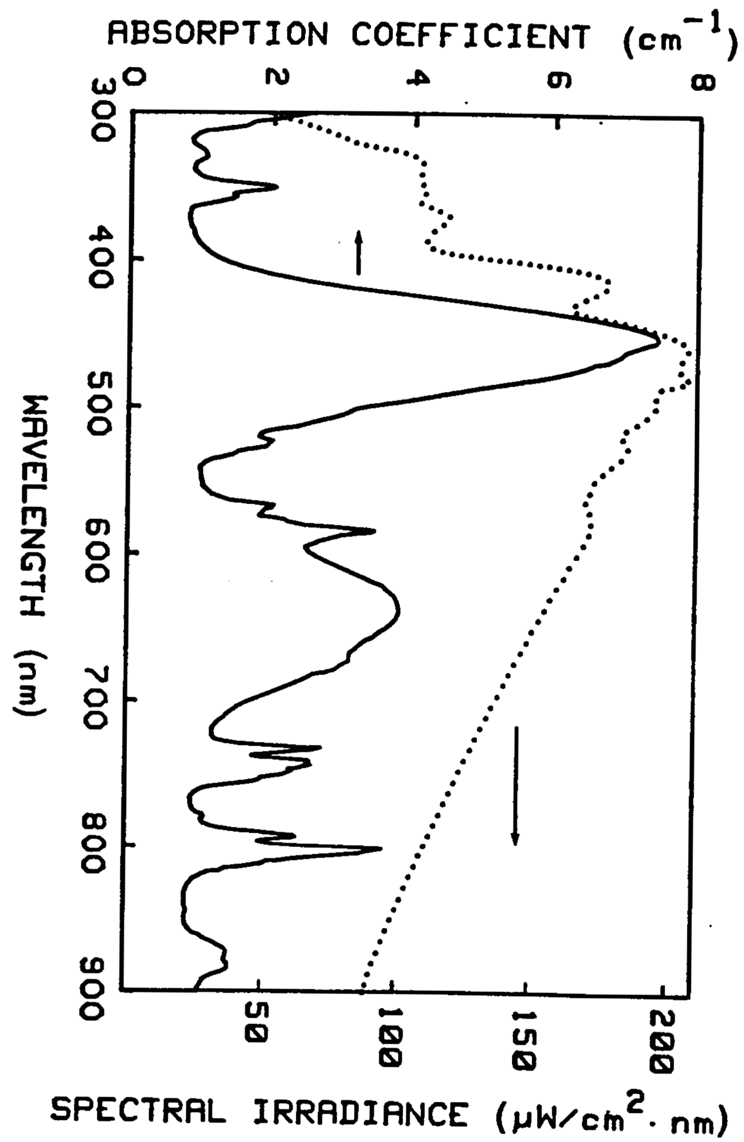

ABSORPTION COEFFICIENT (cm⁻¹)
0
2
4
6
8
300
400
500
600
700
800
900
WAVELENGTH (nm)
50
100
150
200
SPECTRAL IRRADIANCE (μW/cm²· nm)

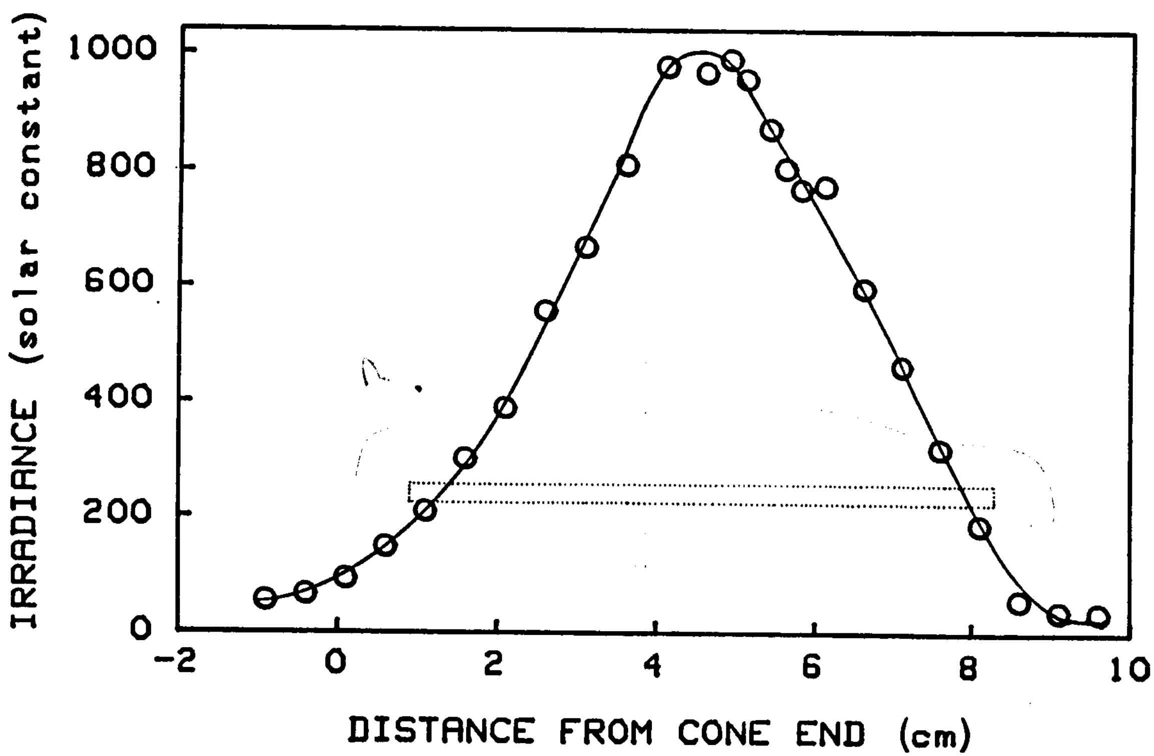
IRRADIANCE (solar constant)
0
200
400
600
800
1000
-2
0
2
4
6
8
10
DISTANCE FROM CONE END (cm)

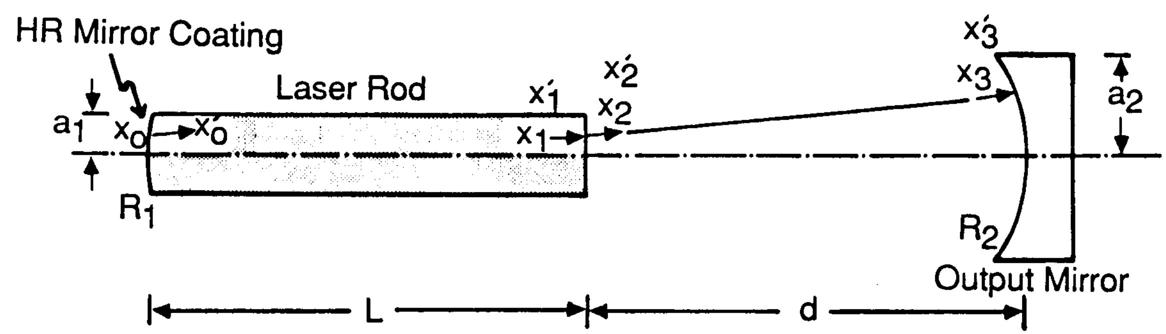
HR Mirror Coating
Laser Rod
a1
x0
x0'
R1
x1'
x1
x2'
x2
x3'
x3
a2
R2
Output Mirror
L
d